



Global-scale characterization of turning points in arid and semi-arid ecosystem functioning

Bernardino, Paulo N.; De Keersmaecker, Wanda; Fensholt, Rasmus; Verbesselt, Jan; Somers, Ben; Horion, Stephanie

Published in:
Global Ecology and Biogeography

DOI:
[10.1111/geb.13099](https://doi.org/10.1111/geb.13099)

Publication date:
2020

Document version
Publisher's PDF, also known as Version of record

Document license:
[CC BY](#)

Citation for published version (APA):
Bernardino, P. N., De Keersmaecker, W., Fensholt, R., Verbesselt, J., Somers, B., & Horion, S. (2020). Global-scale characterization of turning points in arid and semi-arid ecosystem functioning. *Global Ecology and Biogeography*, 29(7), 1230-1245. <https://doi.org/10.1111/geb.13099>



RESEARCH PAPER

Global Ecology
and BiogeographyA Journal of
Microecology

WILEY

Global-scale characterization of turning points in arid and semi-arid ecosystem functioning

Paulo N. Bernardino^{1,2} | Wanda De Keersmaecker¹ | Rasmus Fensholt³ |
Jan Verbesselt² | Ben Somers¹ | Stéphanie Horion³

¹Division Forest, Nature and Landscape, KU Leuven, Leuven, Belgium

²Laboratory of Geo-Information Science and Remote Sensing, Wageningen University, Wageningen, The Netherlands

³Department of Geosciences and Natural Resource Management (IGN), University of Copenhagen, Copenhagen, Denmark

Correspondence

Paulo N. Bernardino, Division Forest, Nature and Landscape, KU Leuven, Celestijnenlaan 200E, 3001 Heverlee, Leuven, Belgium.
Email: paulo.bernardino@gmail.com

Funding information

Federaal Wetenschapsbeleid, Grant/Award Number: SR/00/339; Fonds Wetenschappelijk Onderzoek, Grant/Award Number: REFORCE

Editor: Thiago Silva

Abstract

Aim: Changes in dryland ecosystem functioning are threatening the well-being of human populations worldwide, and land degradation, exacerbated by climate change, contributes to biodiversity loss and puts pressures on sustainable livelihoods. Here, abrupt changes in ecosystem functioning [so-called turning points (TPs)] were detected using time series of Earth observation data. Hotspot areas of high TP occurrence were identified, observed changes characterized and insights gained on potential drivers for these changes.

Location: Arid and semi-arid regions.

Time period: 1982–2015.

Methods: We used a time series segmentation technique (breaks for additive season and trend) to detect breakpoints in rain-use efficiency as a means of analysing changes in ecosystem functioning. A new typology to characterize the detected changes was proposed and evaluated, at regional to local scales, for a set of case studies. Ancillary data on population and drought were used to provide insights on potential drivers of TP occurrence.

Results: Turning points in ecosystem functioning were found in 13.6% (c. 2.1×10^6 km²) of global drylands. Turning point hotspots were primarily observed in North America, the Sahel, Central Asia and Australia. In North America, the majority of TPs (62.6%) were characterized by a decreasing trend in ecosystem functioning, whereas for the other regions, a positive reversal in ecosystem functioning was prevalent. Further analysis showed that: (a) both climatic and anthropogenic pressure influenced the occurrence of TPs in North America; (b) Sahelian grasslands were primarily characterized by drought-induced TPs; and (c) high anthropogenic pressure coincided with the occurrence of TPs in Asia and Australia.

Main conclusions: By developing a new typology targeting the categorization of abrupt and gradual changes in ecosystem functioning, we detected and characterized TPs in global drylands. This TP characterization is a first crucial step towards understanding the drivers of change and supporting better decision-making for ecosystem conservation and management in drylands.

This is an open access article under the terms of the Creative Commons Attribution License, which permits use, distribution and reproduction in any medium, provided the original work is properly cited.

© 2020 The Authors. Global Ecology and Biogeography published by John Wiley & Sons Ltd

KEYWORDS

arid regions, ecosystem functioning, human–natural system, land degradation, rain-use efficiency, remote sensing, segmented trend analysis, semi-arid regions, turning point

1 | INTRODUCTION

Drylands cover c. 40% of the land surface of the Earth and support roughly one-third of the global human population (Millennium Ecosystem Assessment, 2005). Dryland ecosystems are, however, highly susceptible to changes in their dynamics owing to extreme and/or persistent dry years (Barbier, Coutron, Lejoly, Deblauwe, & Lejeune, 2006; Fensholt et al., 2012; Rice, Matzner, Byer, & Brown, 2004) or human perturbations (Barbier et al., 2006; Reynolds et al., 2007). Persistent pressure on those ecosystems may trigger profound alterations in their functioning (Ponce-Campos et al., 2013), ultimately leading to land degradation and desertification. Recent estimates claim that 75% of the land area of the Earth is already degraded, and >90% could become degraded by 2050 (Scholes et al., 2018), notably as a result of climate change (Easterling et al., 2000).

The term “ecosystem functioning” refers to a state or trajectory of a system that accounts for the totality of complex interactions occurring inside it and caused by internal or external drivers (Jax, 2005). Alterations in the way dryland ecosystems function can take place abruptly, instead of gradually (Berdugo, Kéfi, Soliveres, & Maestre, 2017; Scheffer, Carpenter, Foley, Folke, & Walker, 2001). Those abrupt changes can happen either when a disturbance is strong enough to push the system to another state of functioning or when the system surpasses a threshold of environmental conditions and, consequently, cannot maintain its previous way of functioning (Scheffer et al., 2001). Here, we consider these abrupt changes as tipping points when there are reinforcing feedbacks maintaining the system at a certain functioning state (Lenton et al., 2008) or as turning points (TP) when the functioning changes significantly but not necessarily in an irreversible manner (Horion et al., 2016). Following this definition, a tipping point represents an extreme case of a TP.

Both TPs and tipping points in ecosystem functioning may have severe economic and ecological consequences, particularly in drylands (Millennium Ecosystem Assessment, 2005). When a dryland system shifts abruptly from a functional (e.g., being a source of forage) to a degraded state, the livelihoods of the inhabitants are threatened, which can result in increased poverty and food insecurity (Berdugo et al., 2017; Millennium Ecosystem Assessment, 2005). It is therefore essential to monitor such abrupt changes. Although vegetation dynamics (e.g., changes in vegetation activity throughout time) and shifts in vegetation trends have already been addressed in global drylands (de Jong, Verbesselt, Schaepman, & de Bruin, 2012; de Jong, Verbesselt, Zeileis, & Schaepman, 2013; Fensholt et al., 2012), few studies have used an ecosystem functioning approach to do so (e.g., Horion et al., 2016, 2019; Ponce-Campos et al., 2013).

Characterization of TPs at large spatial scales is hampered mostly by the lack of long-term, temporally continuous and

consistent field observations that can be scaled beyond the plot level. Time series of remotely sensed satellite imagery emerge as a viable solution (de Jong et al., 2012; De Keersmaecker et al., 2015; Tian et al., 2015), which can ideally be combined with ground-based information (Horion et al., 2016). However, conventional Earth observation indices [e.g., the normalized difference vegetation index (NDVI); Tucker, 1979] alone may not be optimal for assessing ecosystem functioning in drylands, because productivity in those regions is controlled significantly by precipitation (Herrmann, Anyamba, & Tucker, 2005; Hickler et al., 2005). Therefore, NDVI trend changes may simply reflect variations in inter-annual rainfall dynamics, bearing little information about changes in ecosystem functioning.

The rain-use efficiency (RUE; Le Houérou, 1984), a key indicator for measuring the response of plant production to precipitation, is derived by calculating the ratio between net primary productivity (NPP) and precipitation. Given that precipitation is the main climate constraint to vegetation growth in arid and semi-arid areas, a basic assumption involved when using RUE for characterization of ecosystem changes is that there is an ecosystem-specific relationship between NPP and precipitation (Fensholt et al., 2013; Prince, Wessels, Tucker, & Nicholson, 2007). As such, RUE has been used as a key proxy for assessing ecosystem functioning (Horion et al., 2016; Huxman et al., 2004), land degradation (Fensholt et al., 2013; Prince et al., 2007) or ecosystem resilience (Ponce-Campos et al., 2013). Indications of an altered ecosystem response to hydroclimatic conditions may be inferred from the analyses of temporal changes in RUE. For example, when an ecosystem is degraded and species loss happens, its productivity declines, which has severe implications for the functioning of this ecosystem and is reflected by a decrease in RUE (Chapin et al., 2000; Fensholt et al., 2013). Extreme droughts may also cause a decrease in RUE, suggesting that the ecosystem coping mechanism has reached its limit (Ponce-Campos et al., 2013) and that the ecosystem productivity has been impacted significantly (Horion et al., 2016, 2019). The detection of major breakpoints in RUE time series indicates that the ecosystem response to precipitation has changed significantly through time and, ultimately, enables in-depth analysis of TPs in ecosystem functioning in both anthropogenic and natural landscapes (Horion et al., 2016).

A first study mapping TPs in drylands was made at the regional scale (Horion et al., 2016), but no global-scale analysis has been attempted so far. Thus, the general objective of this study was to provide a general synthesis of changes in the ecosystem functioning of drylands at the global scale by mapping and characterizing TPs. We focused on three specific research questions:

1. Which global dryland regions were hotspots of altered ecosystem functioning during recent decades?

2. What types of major changes in functioning occurred in those regions, and when did the TP take place?
3. How may human-induced pressure and climate extremes affect the occurrence of TPs?

Considering that abrupt changes in RUE indicate TPs in ecosystem functioning, we assumed that areas with a high spatial concentration of TPs represented hotspot regions of altered functioning. Here, we used breaks for additive season and trend (BFAST; de Jong et al., 2012, 2013; Verbesselt, Hyndman, Newnham, & Culvenor, 2010), which is a time series segmentation technique able to assess gradual and abrupt changes in RUE. Moreover, explicit information on the rate of change in RUE would allow us to gain a better understanding of changes in functioning over time. Thus, we developed a new typology for categorizing TPs, optimized for characterizing the behaviour of the ecosystem before and after TPs and also taking into account alterations in the rate of change. Lastly, ancillary data on population density and climate extremes were used to provide insights into the determinants of hotspots of change.

2 | MATERIALS AND METHODS

2.1 | Study area

Drylands encompass regions where the production of crops, forage and other ecosystem services are limited by water (Millennium Ecosystem Assessment, 2005). Köppen's classification (Peel, Finlayson, & McMahon, 2007) was used to define our study area, encompassing drylands with arid and semi-arid climates. Although hyper-arid and dry sub-humid regions might also be considered drylands, these were not included in our analysis. Hyper-arid regions are mainly not vegetated, whereas in dry sub-humid regions precipitation might not be the dominant limiting factor (Nemani et al., 2003), making RUE an inadequate indicator of ecosystem functioning (Horion et al., 2016).

2.2 | Dataset on ecosystem functioning of global drylands

To characterize temporal changes in ecosystem functioning (expressed here as changes in RUE), we used long-term time series of remotely sensed estimations of NDVI and rainfall. The NDVI, the normalized ratio between red and near-infrared reflectance, derived from satellite imagery is a widely used proxy for vegetation density and/or health (Tucker, 1979). Here, we used the third-generation Global Inventory Modeling and Mapping Studies (GIMMS) NDVI from Advanced Very High Resolution Radiometer (AVHRR) sensors version 1 (NDVI3g.v1) dataset (Tucker et al., 2005), which provides bi-monthly data at 0.083° spatial resolution ranging from July 1981 to December 2015. A median NDVI value of .1 was used as the threshold to remove areas with sparse/absent vegetation (de Jong et al., 2013). Moreover, areas covered by snow and deserts were

excluded using the Moderate Resolution Imaging Spectroradiometer Land Cover product (MCD12C1) for 2012, at 0.05° spatial resolution (Friedl & Sulla-Menashe, 2015). Precipitation data were obtained from the Climate Hazards Group InfraRed Precipitation with Station data (CHIRPS) dataset, which provides monthly data spanning from 1981 to 2015 at 0.05° resolution (Funk et al., 2015). We resampled the CHIRPS data to match the spatial resolution of the NDVI3g.v1 dataset using the nearest neighbor method.

Rain-use efficiency is derived by dividing NPP by precipitation. Here, we used the growing season NDVI small integral values, which represent the sum of the "greenness" during the growing season and can therefore be related directly to vegetation productivity, as a proxy of NPP (Fensholt et al., 2013). The NDVI small integral values in drylands usually range from 0.029 to 1.361 (10th and 90th percentiles, respectively, of the average NDVI small integral values between 1982 and 2015). They were extracted for each year between 1982 and 2015 using TIMESAT (Jönsson & Eklundh, 2004), using the same settings as the ones specified by Horion et al. (2016) (Supporting Information Table S1). Areas with double growing seasons were included by considering two separate NDVI small integral values for each year.

For estimates of precipitation, we used the sum of precipitation data during the growing season months (as determined by the NDVI analysis). As dryland vegetation may respond to precipitation with variable time-scales (Horion, Cornet, Erpicum, & Tychon, 2013; Vicente-Serrano et al., 2013), multiple time spans for computing the precipitation sum were tested. Specifically, we calculated the precipitation sum over n months before the start of the growing season until the end of the growing season, with n ranging from zero to 12. For each pixel, the time span that showed the highest correlation between the NDVI integral and the precipitation sum was selected as the optimal time span. Optimal precipitation sums were then estimated per pixel and RUE time series generated. One of the basic assumptions when interpreting temporal changes in RUE as being non-climate related is that the RUE time series is statistically independent of the precipitation inputs (Fensholt et al., 2013). To test this assumption, we regressed (pixel-wise) the RUE data against precipitation sums. Turning points detected in pixels that showed a significant relationship ($p < .05$) indicated that driver attribution should be interpreted with caution.

2.3 | Characterization of changes in ecosystem functioning

To detect and characterize changes in ecosystem functioning, BFAST was applied on RUE time series. BFAST decomposes time series into trend, seasonal and remainder components using a piecewise linear trend and seasonal model, and detects abrupt changes in the trend and seasonal components (Verbesselt et al., 2010). More specifically, BFAST01, a variant of BFAST that allows detection of the major breakpoint (none or one) was implemented (de Jong et al., 2013). The algorithm not only allows the detection of abrupt changes in functioning (i.e., TPs) but also their characterization. The formula argument of

BFAST01 was set to “response ~ trend”, because we used yearly time series with no seasonality, and several different bandwidth values were used in an incremental fashion, as explained better in the “Confidence of the detected TPs” subsection. Default settings were used for the remaining arguments. The fitted linear trend can be classified, taking into account the existence of an abrupt change in the time series and the slope direction of the detected trends (de Jong et al., 2013).

Application of this classification can already provide information about changes in ecosystem dynamics. Nevertheless, it does not allow (a) the identification of regions where the rate of change varied over time; and (b) ensuring that the trend in functioning of a system has shifted significantly to the opposite direction. Here, we propose an improved typology for BFAST01, which also considers differences in the steepness and significance of the trends before and after the detected breakpoint. This allows for an improved qualification of the rate of change in the ecosystem (i.e., slowing down or accelerating) and the status of shifts in the trend (i.e., transitional or complete).

As a result, the improved typology consists of six types describing the overall trends and trend shifts and four subtypes providing a more detailed view on the rate and significance of changes (Table 1). Detailed information about the new typology can be found in the Supporting Information (Appendix S1). All analyses were implemented in the R environment (R Core Team, 2018), and the script with the new typology function is already available (see “Data accessibility” section).

2.4 | Confidence of the detected turning points

In order to identify regions with high/low confidence in the detected TPs, we developed the turning point occurrence index (TPOI). The bandwidth parameter of the BFAST01 function determines the size of the data window, relative to the sample size, that will be used by the moving sum of residuals test (de Jong et al., 2013). This means that changing the bandwidth value modifies the break detection capacity of the algorithm, meaning that certain values (i.e., intermediate values) will result in easier detection of breaks. We thus applied the BFAST01 to the RUE data with bandwidth values ranging from the minimum to the maximum allowed by the length of the time series (i.e., from 2/34 to 33/34). By summing, pixel-wise, the number of times a TP was detected for all possible bandwidth values and dividing it by the maximum possible number of detected breaks (32), we obtained the TPOI. A high TPOI value indicated that, even when the algorithm specifications made it harder for BFAST01 to detect a break, the TP was detected, meaning that there was a high chance that the TP truly occurred.

2.5 | Population density and drought versus turning point occurrence

Population pressure and climate extremes are known to be major drivers of changes in dryland ecosystem functioning (Cherlet et al., 2018). We, therefore, analysed the relationships between the occurrence of TPs, population density and drought incidence. This was

achieved by calculating, for each study region, the percentage of pixels showing a TP for different classes of population density and drought occurrence. For estimates of population density (as persons per square kilometre), we used the Gridded Population of the World v.4 (GPWv4) Revision 10 dataset for 2015 (Center for International Earth Science Information Network, 2017). The standardized precipitation evapotranspiration index (SPEI) 9 month dataset was used for estimates of drought (Vicente-Serrano, Beguería, López-Moreno, Angulo, & El Kenawy, 2010). To identify hotspots of drought occurrence, we counted the number of abnormally dry months (i.e., SPEI values ≤ -1.5 , representing moderate to extreme drought conditions) during the growing seasons between 1982 and 2015.

Global drylands were separated into focal regions: North America, the Sahel, Asia and Australia. South America was not considered here owing to a lack of large-scale TP events. All pixels were divided into four population density and drought occurrence classes, from very low to very high density/occurrence (Table 2), and a cross-tabulation approach was used. For each region, population density quartiles were used to create classes of equal size (Table 2). This improved the region-specific characterization of population density pressure over ecosystems, because population density varies greatly among regions. Classes of drought occurrence were assigned using the same rationale, with quartiles of drought frequency estimated for global drylands (and not focal regions) because the SPEI is normalized per pixel (Table 2). Lastly, the percentage of pixels that presented a TP was plotted for the combinations of population and drought classes, providing insights about the relationship between each driver (or combination of drivers) and TPs for each region.

Moreover, to characterize the different combinations of population/drought classes further, we calculated the fraction of pixels assigned to major land-cover types (according to the MCD12C1) for each combination. This provided additional information to support the driver attribution analysis. Land-cover types that resulted in <1% cover for each of the possible combinations of population and drought classes were excluded.

2.6 | Case studies

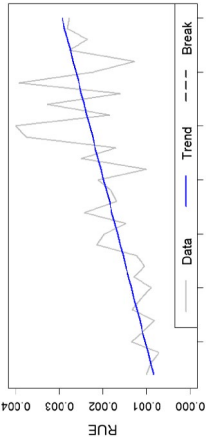
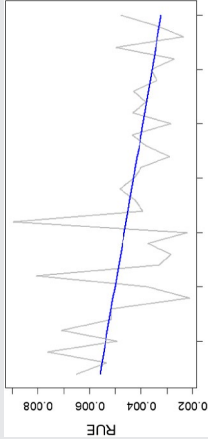
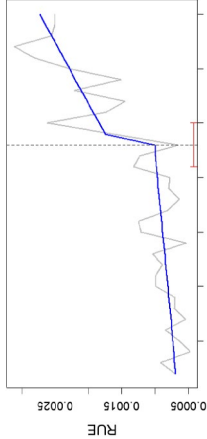
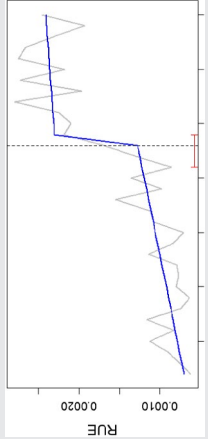
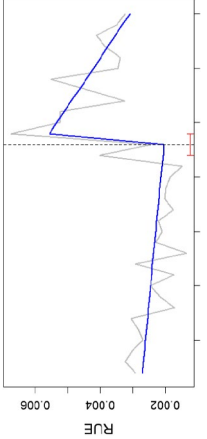
Changes in ecosystem functioning were analysed further over four case studies. Within each focal region, we identified a hotspot area of changes and selected a case study based on its spatial extent and the type of TP detected. Results from the new typology were then analysed in scrutiny and based on literature, aiming to confirm the results of our categorization for these areas.

3 | RESULTS

3.1 | Hotspots of turning point occurrence





The new BFAST01 typology was applied on improved RUE estimates (i.e., calculated by considering the lagged effect of vegetation response

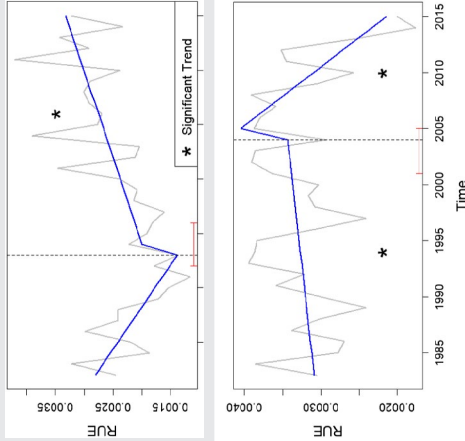
TABLE 1 Typology of types and subtypes of changes in ecosystem functioning

Type	Subtype	Example	Illustration of ecological inference
Stable increase	No subtype		Gradual increase in ecosystem functioning owing to increased temperature or CO ₂ fertilization (e.g., Horion et al., 2016)
Stable decrease	No subtype		Gradual land degradation, such as long-term loss of soil organic matter content (e.g., Horion et al., 2019)
Interrupted increase	Accelerating		Shift in species composition towards a faster increase in ecosystem functioning (e.g., Chapin et al., 2000)
Interrupted increase	Slowing down		Shift in species composition towards a slower increase in ecosystem functioning (e.g., Chapin et al., 2000)
Interrupted decrease	Accelerating		Extreme drought leads to high RUE, but subsequent plant mortality decreases ecosystem productivity by reducing vegetation density (e.g., Latsch et al., 2005)

(Continues)

TABLE 1 (Continued)

Type	Subtype	Example	Illustration of ecological inference
	Positive reversal 	Transition	Cropland abandonment, followed by natural regeneration of vegetation (e.g., Horion et al., 2016; present study)
	Negative reversal 	Complete	Deforestation, leading to a decrease in ecosystem functioning in north-eastern Brazil



Note: Examples based on rain-use efficiency (RUE) time series are presented, representing different types of major changes in ecosystem functioning. Examples of the potential ecological inference of the observed changes are given. In addition, the last time series, which shows a negative reversal, was extracted from a region that underwent intense deforestation in the 2000s in Brazil (state of Piauí). The vegetation states before and after deforestation are presented as true colour satellite images in the Supporting Information (Figure S4). The grey line represents the RUE time series and the blue line the fitted linear model. The dotted vertical line represents the year of the detected turning point (TP), with the red mark indicating the confidence interval for the estimated timing of the TP. The asterisks indicate that the fitted trend is significant ($p < .05$). The colours used to illustrate each type and subtype are identical to the colours used in the maps produced. Note that not all possible combinations of types and subtypes are presented here.

TABLE 2 Ranges of values used to aggregate the pixels into classes of very low, low, high and very high population density/drought occurrence

Class	Population density (persons/km ²)				Drought occurrence (months)
	North America	Sahel	Asia	Australia	All regions
Very low	<0.03	<9.98	<1.48	<0.002	<9
Low	0.03–0.19	9.98–20.96	1.48–12	0.002–0.004	9–15
High	0.19–1.78	20.96–48.48	12–58.5	0.004–0.013	16–24
Very high	>1.78	>48.48	>58.5	>0.013	>24

Note: Population density intervals were defined region-wise, but the same drought occurrence intervals were used for all the regions.

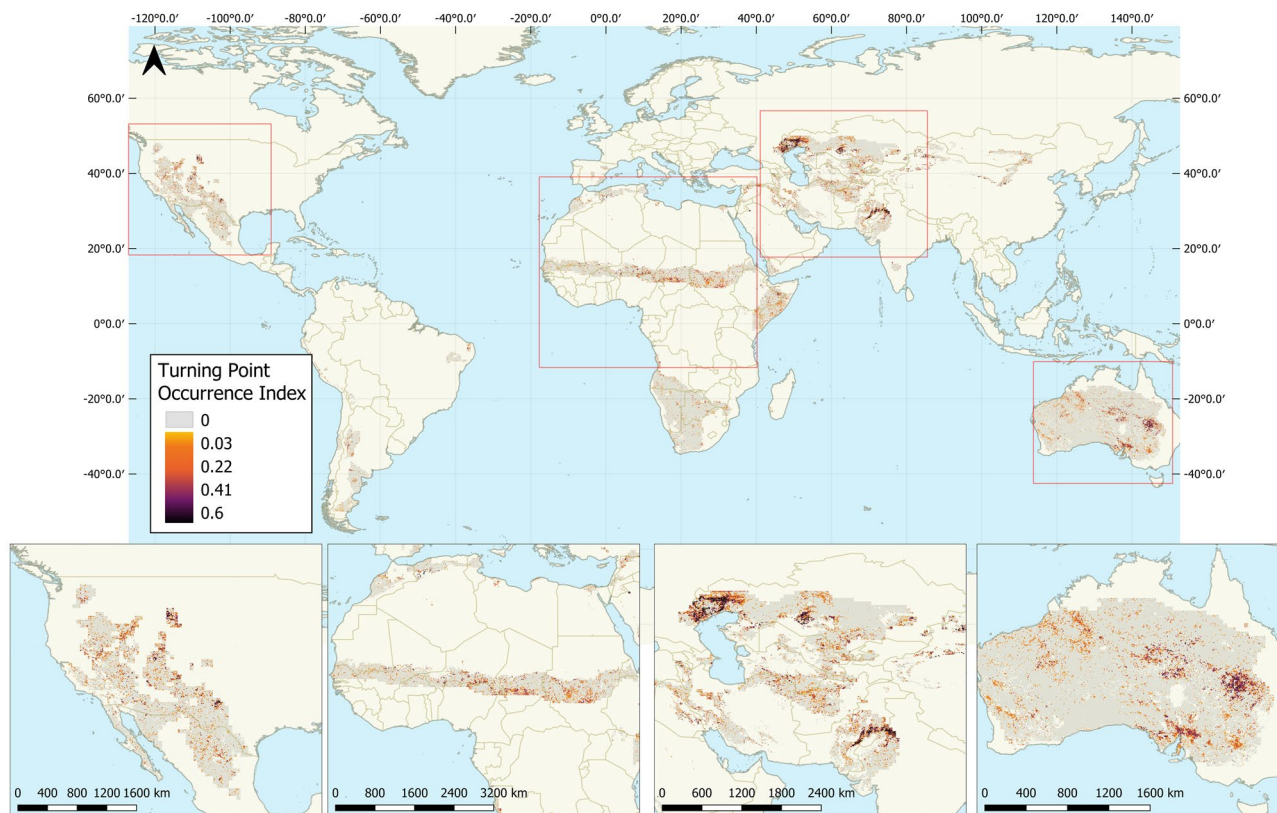


FIGURE 1 Turning point occurrence index (TPOI) map. Darker colours represent areas with a higher certainty of the occurrence of a turning point (TP) in ecosystem functioning and its associated timing. Hotspots of TP occurrence are observable, mainly in the highlighted regions (i.e., central-western North America, the Sahel, north-western Central Asia and Australia) [Colour figure can be viewed at wileyonlinelibrary.com]

to precipitation) to detect and categorize TPs in the ecosystem functioning of drylands. The TPOI revealed regions of global drylands with a high (spatial) occurrence of TPs during recent decades and high confidence for the detected TPs (Figure 1). Those regions were central-western North America, the Sahel, north-western Central Asia and Australia. Hereafter, we refer to those regions as “focal regions”.

It is noteworthy that, by considering the lagged vegetation response to precipitation in the RUE estimation, the number of detected TPs increased by 22.4% when compared with using the growing season precipitation sum without added months. However, some areas still showed a heavy influence of variability in precipitation on RUE data (Supporting Information Figure S1).

3.2 | Characterization of the detected turning points

Overall, the total share of global drylands showing TPs was relatively limited (13.6%, which corresponds to $c. 2.1 \times 10^6$ km²). No significant ($p < .05$) change in RUE was seen in 53.3% of global drylands, and an additional 33.1% showed stable changes. Maps with the RUE trend type, subtype and time of TP occurrence for drylands worldwide can be found in the Supporting Information (Figure S2). The dominant types of TPs were positive reversal (i.e., decrease to increase; 37.9%) and interrupted increase in RUE (23.3%), followed by interrupted decrease and negative reversal (i.e., increase to decrease; 21.4% and 17.3%, respectively). The analysis of the subtypes of TPs

revealed a dominance of accelerating rates of change regardless of the direction of change (i.e., 71.5% of the pixels classified as interrupted increase and 69.4% as interrupted decrease were assigned to the “accelerating” subtype). In addition, both positive and negative reversals were mostly assigned to the “transition” subtype (81.5% and 75.2%, respectively).

The relative occurrence of each ecosystem change type and subtype varied greatly between focal regions (Figures 2 and 3a). In North America, the most common TPs were interrupted decrease with acceleration after the TP (23.31% of the pixels with a TP) and

negative reversal in a transitional state (27.2%; Figure 3a). On the contrary, the most common pattern of change in the Sahel was positive reversal in RUE (53.72%; Figure 3a). The same predominance was observed in Asia and Australia (40.35% and 47.51%, respectively; Figure 3a). Turning points were detected between 1987 and 2010, with a high frequency of TPs in 1992 observed in the Sahel and Australia (Figures 2 and 3b). Given that the structural change test performed by BFAST01 does not allow for the detection of TPs close to the start or end of the time series (de Jong et al., 2013), no TPs were detected before 1987 or after 2010.

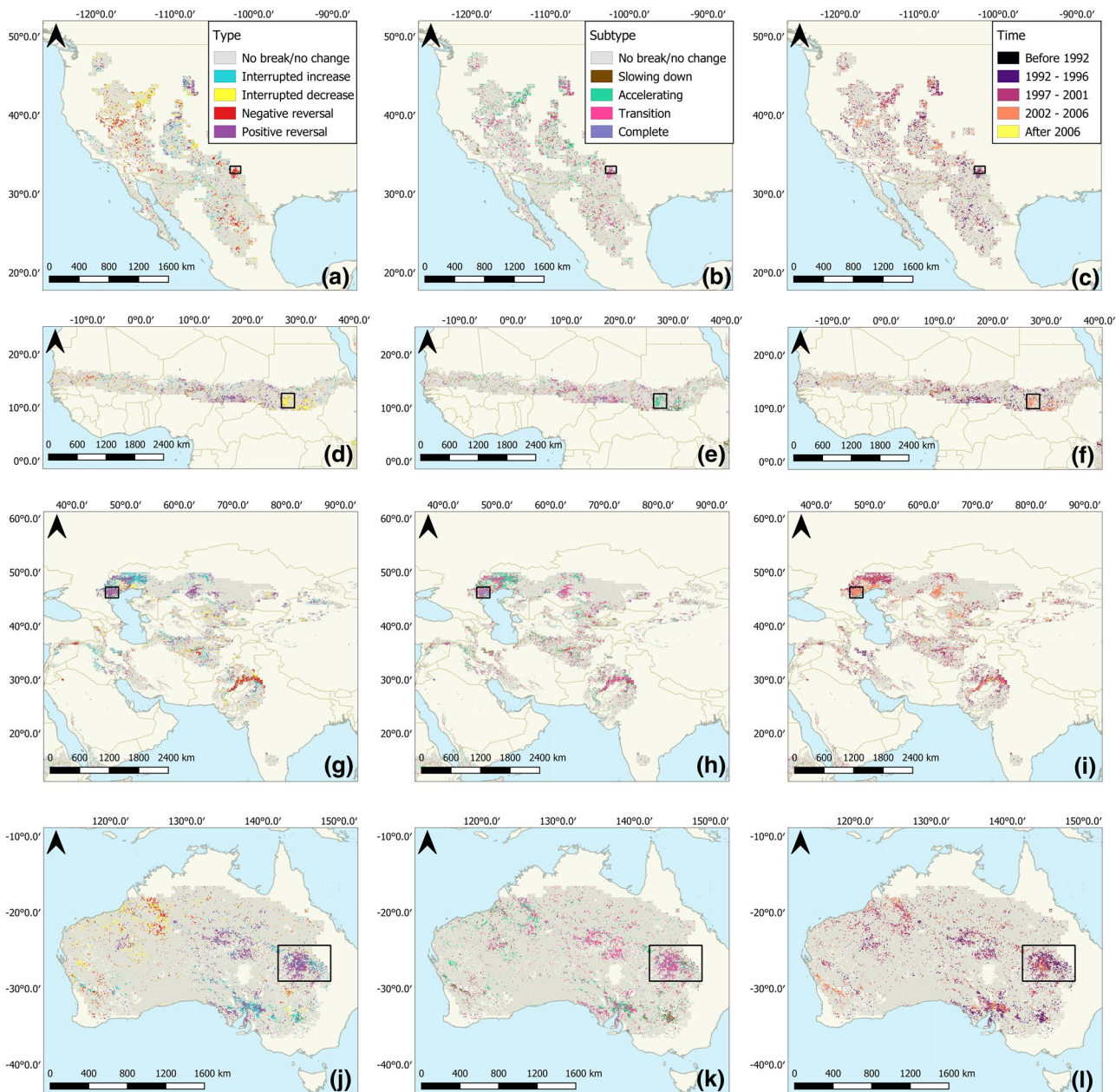


FIGURE 2 Type, subtype and time of occurrence of turning points (TPs) in ecosystem functioning over the four focal regions, which are North America (a–c), the Sahel (d–f), Central Asia (g–i) and Australia (j–l). Areas used as case studies are highlighted with black rectangles and represented in greater detail in Figure 6 [Colour figure can be viewed at wileyonlinelibrary.com]

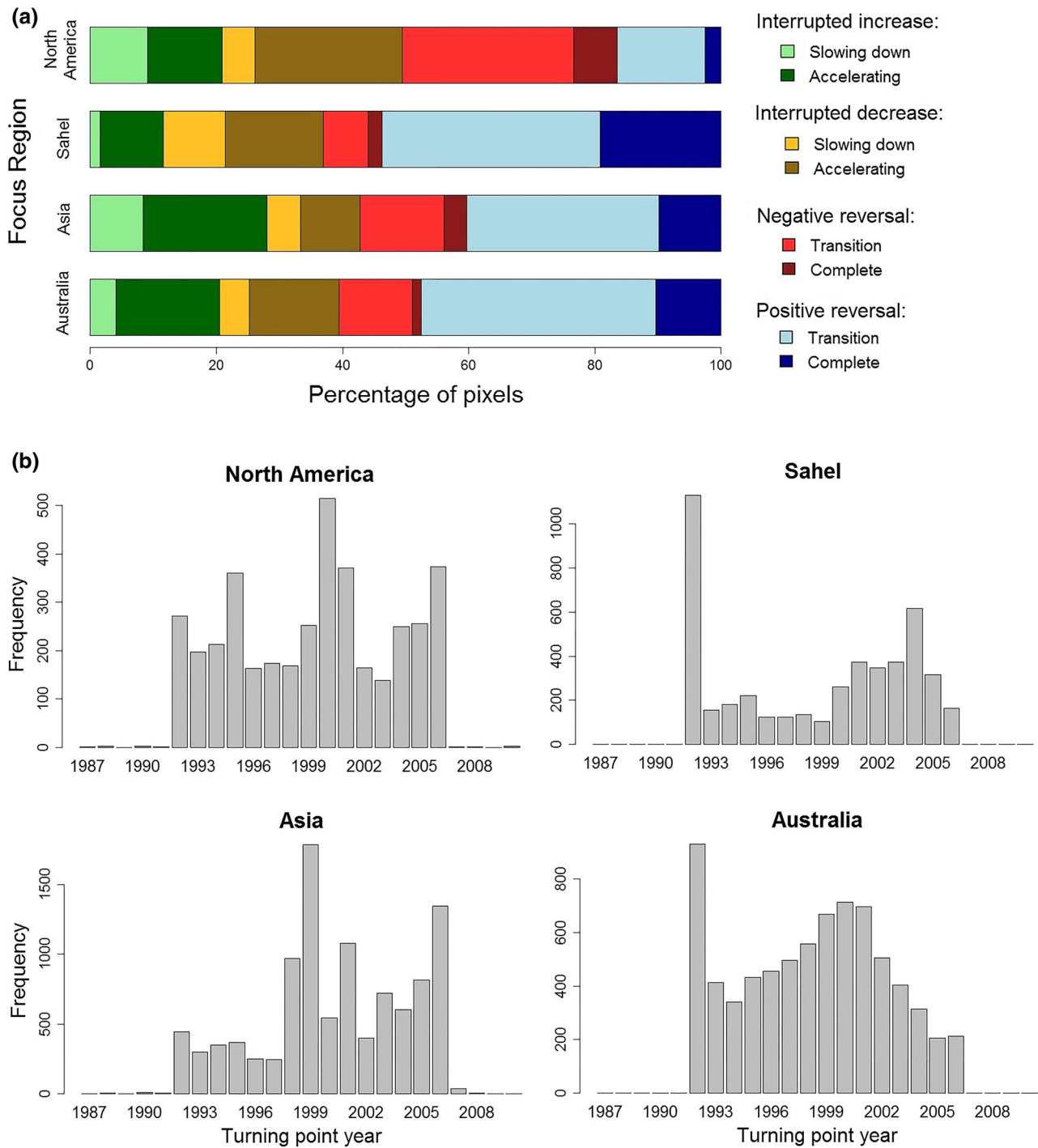


FIGURE 3 Turning points (TPs) in ecosystem functioning (subtype) and year of occurrence, for each focal region. (a) The percentage of pixels for each possible combination of type and subtype. (b) The frequency of TPs detected in each year, from 1987 to 2010 [Colour figure can be viewed at wileyonlinelibrary.com]

3.3 | Population density and droughts versus turning point occurrence

In North America, higher drought pressure was related to high TP occurrence (Figure 4a). In addition, TPs did not occur more frequently over a specific land-cover type, because North American drylands present a shared dominance of grasslands and shrublands

(Figures 4a and 5a–c). In the Sahel, the highest percentages of TPs also occurred under high to very high drought pressure (Figure 4b). In addition, fewer TPs were observed where more croplands were present and drought was less frequent (Figures 4b and 5f). In Asia, a particularly high percentage of TPs (34.07%) was observed where population pressure was very high and drought occurrence very low (Figure 4c). This combination of classes was dominated by croplands

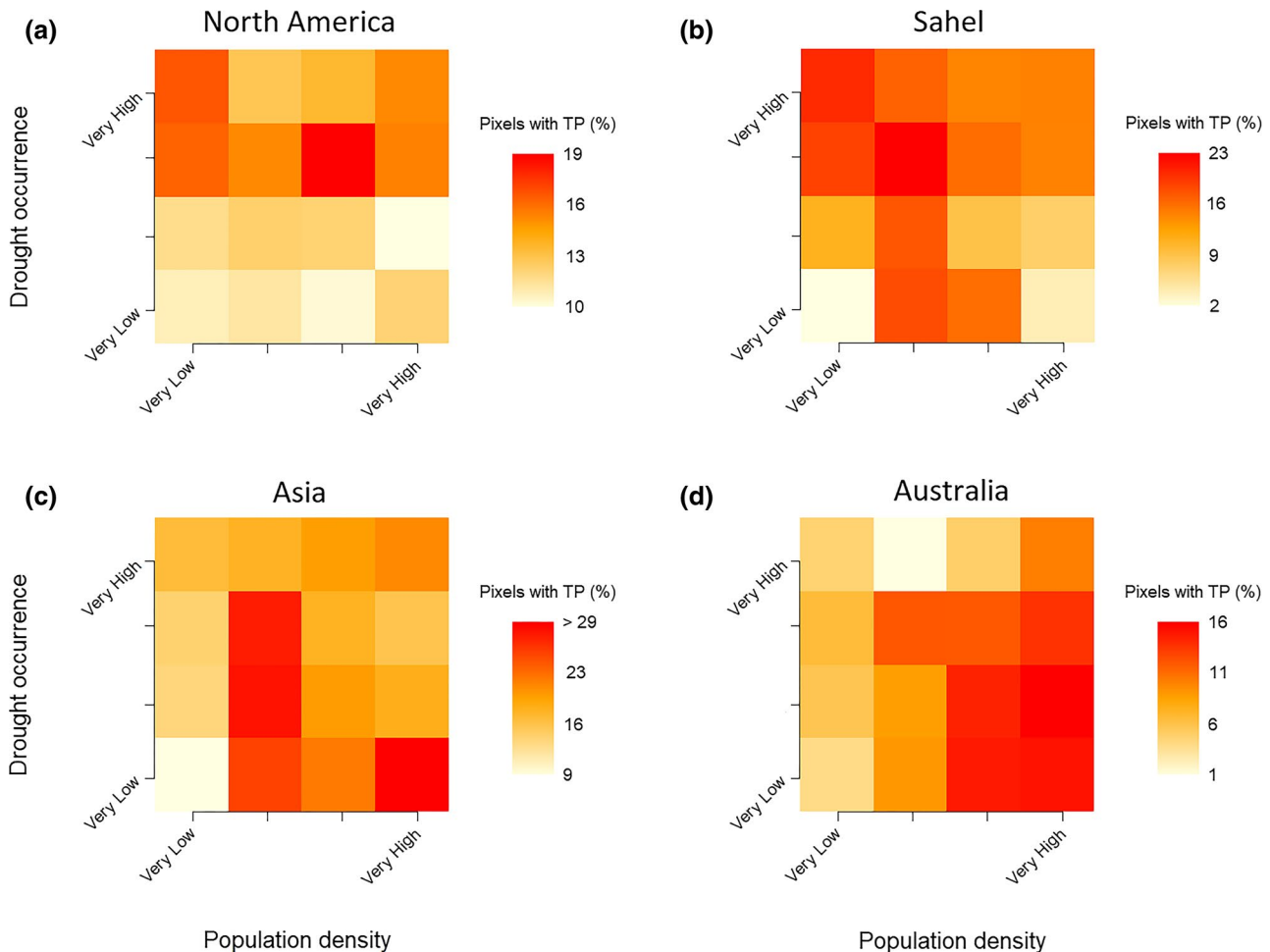


FIGURE 4 Percentage of pixels showing a turning point (TP) for different classes of population density and drought occurrence. For each region, the minimum and maximum percentages were used to set the limits of the colour range, in order to avoid overshadowing of within-region differences [Colour figure can be viewed at wileyonlinelibrary.com]

(Figure 5i). Lastly, in Australia, TPs occurred more frequently where population pressure was high (Figure 4d).

3.4 | Case studies

The four selected sites were used to evaluate the new proposed typology in more details (Figure 6; Supporting Information Figure S3). The sites were located in western Texas (USA; Figure 6a–c), the south of Sudan (Sahel; Figure 6d–f), the north-west of the Caspian Sea (Eurasia; Figure 6g–i) and the Mulga Lands (Australia; Figure 6j–l).

In western Texas, reversals from increasing to decreasing trends in functioning were observed over an area of c. 12,150 km² (Figure 6a). Some trends were sub-classified as transitional, whereas others had completely reversed (Figure 6b). The reversal occurred mainly between 1992–1996 and 1999–2001. In the south of Sudan, a large area of c. 25,100 km² was classified as interrupted decrease with acceleration after the TP (Figure 6d,e). The year of TP occurrence was consistent for all pixels (i.e., 2004). North-west of the Caspian Sea, an extensive area of c. 46,400 km² was classified as

reversal from decrease to increase, mostly sub-classified as complete (Figure 6g,h). These TPs occurred mainly between 2002 and 2006 (Figure 6i). The region selected in Australia showed an extensive area classified as positive reversal (Figure 6j,k). Both transitional and complete TPs co-occurred.

4 | DISCUSSION

4.1 | Improved reading of abrupt changes in global drylands

We have provided here the first global-scale assessment of TPs in ecosystem functioning of drylands. Hotspots of altered functioning were identified in central-western North America, eastern Sahel, north-western Central Asia and eastern Australia (Figures 1 and 2). Our results point to 1992 as a key year for observed abrupt changes in Earth observation data, as already reported by previous studies (de Jong et al., 2012; Tian et al., 2015), which identified the eruption of Mount Pinatubo in June 1991 as a potential driver for residual

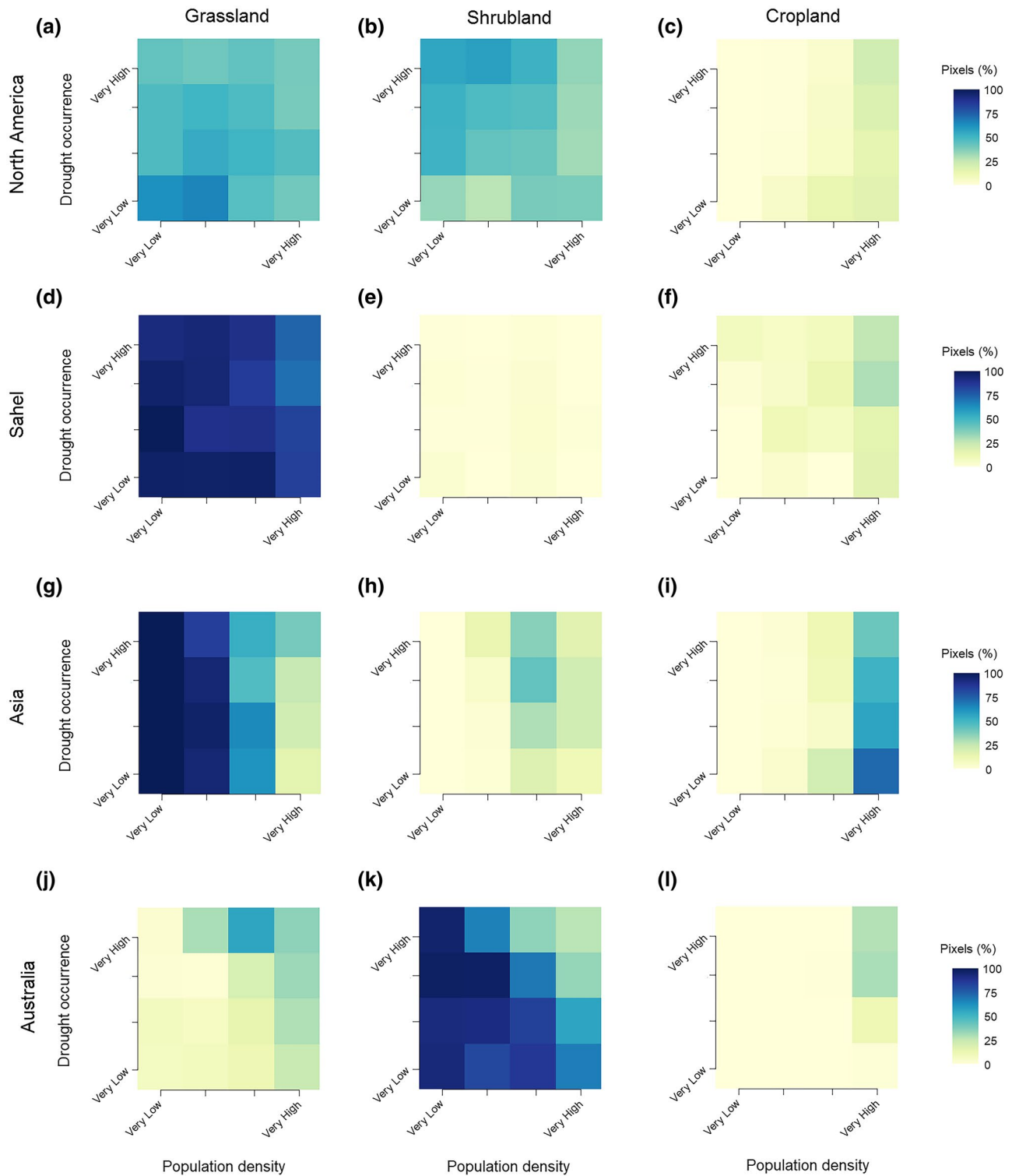


FIGURE 5 Percentage of pixels assigned to distinct land-cover types, for different classes of population density and drought occurrence. Darker colours indicate a higher percentage of pixels for any given land-cover type and combination of population and drought classes. Please note that, for this figure, summing the values for each combination of classes (e.g., very high drought occurrence and population density) inside each region will result in 100% [Colour figure can be viewed at wileyonlinelibrary.com]

shifts in NDVI time series around 1992. However, Tian et al. (2015) demonstrated that, besides being corrected for the influence of volcanic aerosols, the NDVI3g.v1 is the most temporally consistent long-term AVHRR dataset.

The proposed new typology also allowed for a detailed characterization of the detected changes, besides providing information about the year of the TP occurrence (Figures 2, 3 and 6). Our results are generally in line with the study of Horion et al. (2016)

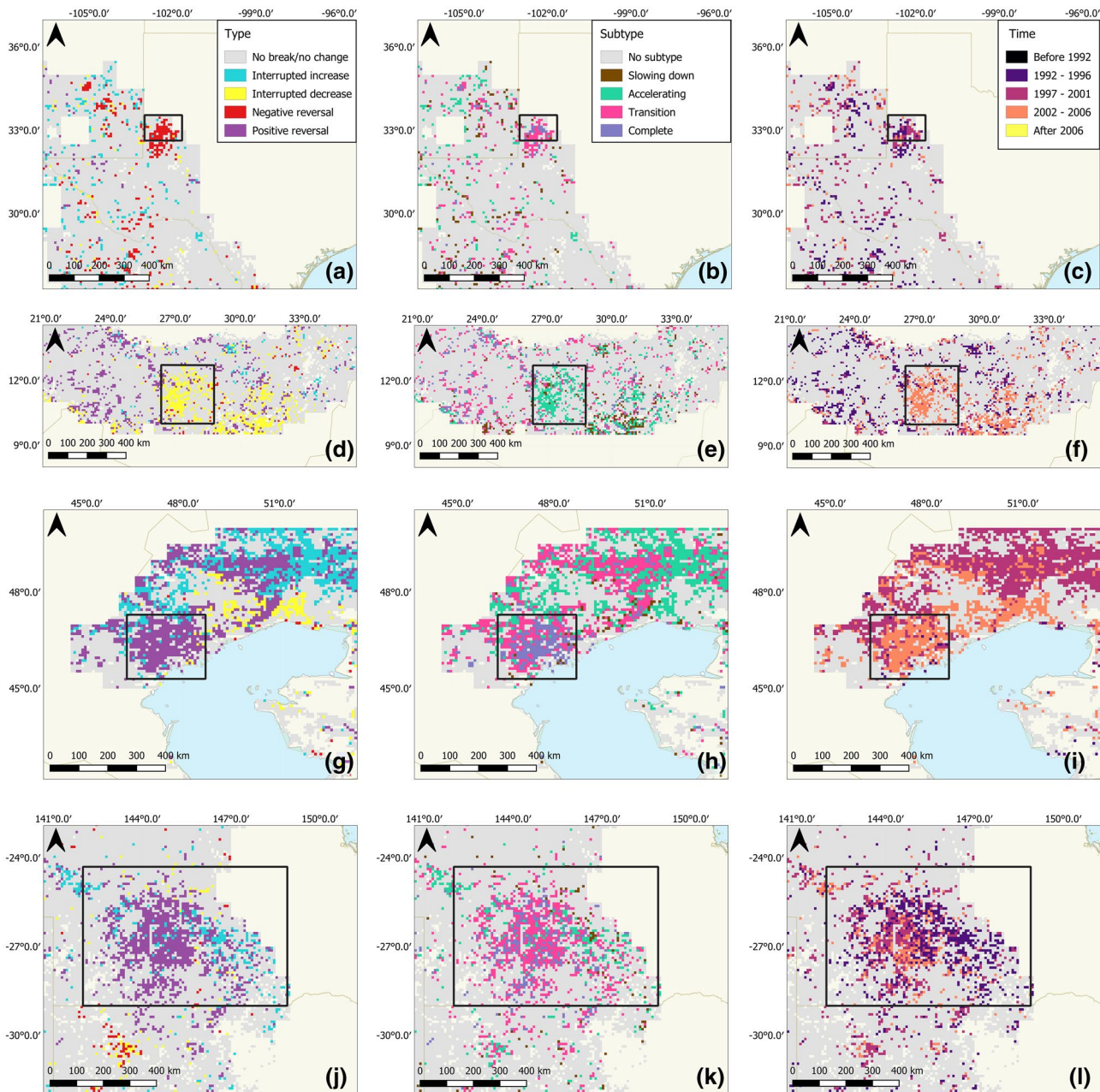


FIGURE 6 Sites selected as case studies for the description and interpretation, based on published studies, of the patterns detected by the typology here proposed. Grey lines are international/regional borders, and black lines delimit the site of the case study (locations of sites are indicated in Figure 2). Maps (a–c) show the case study in North America, located in Texas (USA); maps (d–f) are for the case in the Sahel, located in the southern part of Sudan; maps (g–i) show the case in Central Asia, located north-west of the Caspian Sea; and maps (j–l) represent the case in Australia, which is mostly within the Mulga Lands bioregion [Colour figure can be viewed at wileyonlinelibrary.com]

carried out over northern Eurasia. However, some of the detected TPs differ. The reasons for such differences can be related to data or methods:

1. Regarding the data, although both studies used RUE time series as a proxy for trends in ecosystem functioning, RUE was computed using the NDVI3g.v1 and the CHIRPS datasets in our study, whereas Horion et al. (2016) used the GIMMS Fraction of Absorbed Photosynthetically Active Radiation and the Global Precipitation Climatology Project (GPCP) products for estimates of vegetation and precipitation, respectively.
2. Regarding the methods, we applied an improved typology of changes in ecosystem functioning, which also allowed for quantification of alterations in the rate of change before and after TPs (i.e., accelerating or decelerating trends; see Supporting Information Appendix S1). In addition, we accounted for the lag in the response of vegetation to precipitation before performing the TP detection analysis and used the BFAST01 algorithm in an iterative fashion with increasing bandwidth values in order to detect and assess the TPs. Those two steps substantially increased the number of detected TPs, potentially reducing the number of false negatives in our analysis. Such improvements represent

important steps towards the comprehensive analysis of pathways of change in ecosystem functioning. For example, it was recently shown that local degradation processes (e.g., decreased vegetation productivity owing to soil erosion) would be signalled by a change in the magnitude of the slope, suggesting a slowing down in ecosystem functioning (Horion et al., 2019). Thanks to our new typology, acceleration and slowing down of ecological processes can now be captured and labelled in a systematic way.

4.2 | The new typology under scrutiny

Comprehensive mapping and categorization of changes in ecosystem proxies derived from Earth observation data are important steps towards an improved understanding of changing pressure over dryland ecosystems. Nonetheless, attribution of drivers remains a major challenge in global environmental studies (Rasmussen et al., 2016), notably owing to the diversity of driving forces and the limited number of reference sites suitable for validation (Cherlet et al., 2018). Examples of ecological inference for the types of ecosystem changes are given in Table 1. However, it is important to note that different drivers or combinations of drivers may result in the same type of ecosystem change (Horion et al., 2019). Further research is needed to deepen our knowledge on the variability of ecosystem pathways resulting from single or combined driving forces.

In the present study, we took the first step in that direction by selecting four case studies to assess our new typology further and to investigate potential ecological implications of the observed TPs. Negative reversals in RUE were observed in western Texas (Figure 6a). This site, together with other areas of the Western High Plains, underwent a cycle of cropland abandonment (during the Conservation Reserve Program established in the 1980s) and re-cultivation or conversion to livestock grazing (Drummond et al., 2012; Sullivan et al., 2004). Such institutional change can lead to abrupt changes towards reduced functioning in areas that were previously preserved, that is, shift to a decreasing trend in RUE owing to loss of biodiversity after conversion from natural vegetation to cropland or pasture. The timing of the TPs detected here (i.e., 1992–1996) aligned with the period of re-cultivation (Drummond et al., 2012; Sullivan et al., 2004).

Interrupted decrease with acceleration (after 2004) was observed in the south of Sudan (Figure 6d–f). The driest year in the decade for this region was reported to be 2004 (Elagib, 2013), and it occurred after a prolonged drought period, which might have triggered an even sharper decrease in functioning in some areas (Elagib, 2013; Elagib & Elhag, 2011). Overall, drought decreases productivity of ecosystems by, for example, reducing vegetation density owing to drought-induced plant mortality (e.g., Lotsch, Friedl, Anderson, & Tucker, 2005; Table 1). However, it has been shown that maximum RUE is observed in dry years (Huxman et al., 2004). The large extent of the hotspot area suggests that the observed accelerated decrease in RUE after 2004 was attributable to significant damage

to the ecosystem functioning caused by the long-term and extreme drought conditions (Ponce-Campos et al., 2013). This is also in line with our results (Figure 4b), which showed that drought relates to a large share of TPs in the Sahel.

In western Kazakhstan and adjacent Russian territory, there was a widespread occurrence of positive reversal in ecosystem functioning trends (Figure 6g), pointing to regions that underwent a degradation process in the past but reverted into a functioning recovery in recent years. The occurrence of TPs at such a scale is typical of climate-induced changes. However, in this specific case, such large-scale human-induced occurrence of TPs is very plausible, in light of the geopolitical history of the region. Large-scale de-intensification of agriculture-related activities, together with the abandonment of lands used as pasture, was reported after the collapse of the Soviet Union, leading to a recovery of natural vegetation (de Beurs & Henebry, 2004; Horion et al., 2016). Specifically, over the case study, intensified livestock breeding and agriculture in the region between the 1970s and 1980s led to significant damage to vulnerable steppe ecosystems (Hölzel, Haub, Ingelfinger, Otte, & Pilipenko, 2002; Zonn, 1995). Also, inappropriate irrigation practices resulted in 1.03 million ha of land suffering from salinization (Zonn, 1995). These factors might explain the observed decreasing trend in functioning during the first half of the observation period. After cropland abandonment, the original natural steppe vegetation was able to regenerate (Hölzel et al., 2002; Horion et al., 2016), which might have resulted in an increase in productivity (Table 1). The process is, however, not immediate, and signs of regeneration (here, an increase in RUE) might take more or less time to be detectable depending on the degree of preceding degradation (e.g., Castellano & Valone, 2007).

Finally, positive reversals in ecosystem functioning were observed over a site in the eastern Australian drylands (Figure 6j). This area covers a great part (c. 38.8%) of the Mulga Lands. Although the region is not suitable for agriculture, it has typically been used for livestock grazing (Witt, Noël, Bird, Beeton, & Menzies, 2011). As grazing has been persistent in the region since the second half of the 19th century (Witt, Harrington, & Page, 2009), other factors are likely to be responsible for the observed reversal in the direction of trends. It is well known that drought has had a major impact on Australian ecosystems in recent decades (Rice et al., 2004). Specifically here, increased rainfall was observed at the end of the 1980s, followed by a severe El Niño-induced drought between 1992 and c. 1997 (Rice et al., 2004; Witt et al., 2009). This is in line with our results showing an important share of TPs occurring during these extremely dry years. After 1997, rainfall levels remained above average for several years, which might explain the trend reversal to an increase in functioning observed over the area after the extremely dry years. Indeed, when water availability is not restricting vegetation growth and fire activity (another constraint for vegetation growth in the region) is controlled by fuel removal owing to grazing, the ecosystem is capable of recovering towards an improved functioning (Witt et al., 2009, 2011).

Such large-scale mapping of areas with altered functioning is of great interest for decision-making related to mitigation of and

adaptation to land degradation in drylands (Millennium Ecosystem Assessment, 2005; Scholes et al., 2018). The characterization of the ongoing processes in those areas (e.g., land degradation or restoration) can possibly help to set priorities when taking measures for ecosystem conservation. Although developed to characterize changes in dryland ecosystems, the new typology might also be applicable in different ecosystems worldwide, with the pre-condition of applying it to a proxy that reflects the functioning of the ecosystem under study (Horion et al., 2019). However, adequate validation with case studies is still required to ensure the validity of the approach for other ecosystems, because the interpretation of the results might differ from those inferred from our study in dryland ecosystems.

4.3 | Conclusion

By implementing the new BFAST01 typology, which allowed for an integrated analysis of gradual and abrupt changes in ecosystem functioning in drylands, we successfully: (a) detected hotspots of altered functioning in recent decades; (b) determined when the alteration occurred; and (c) characterized the trends before and after the TP. The introduction of a TPOI improved the robustness of the TP detection approach. Moreover, using climate data together with in situ information on population density, we (d) obtained overall insights into the drivers of changes in functioning at the regional scale and discussed possible causes of change at the local scale by analysing four case studies. With this new approach, we take a crucial step towards large-scale assessment and characterization of abrupt changes in dryland ecosystem functioning. Such methodological development is urgently needed to support decision-making for the conservation of dryland ecosystems and to mitigate further land degradation caused by human and climate-induced changes. Hotspot regions with high TP occurrence deserve special attention, in particular when the ecosystem functioning presents an accelerated decreasing trend or a shift towards a decreasing trend, because such changes may imply a decrease in productivity, species diversity and/or resilience. Future research should focus on the comprehensive attribution and disentanglement of drivers of TPs (e.g., climate or human induced) and on changes in vegetation stability.

ACKNOWLEDGMENTS

The research presented in this paper is funded by the Belgian Science Policy Office in the framework of the STEREOIII program [project U-TURN, Understanding Turning Points in Dryland Ecosystem Functioning (SR/00/339)]. The authors thank the NASA Global Inventory Modeling and Mapping Studies group for producing and sharing the NDVI3g.v1 dataset and the Climate Hazards Group for producing and sharing the CHIRPS dataset. The authors thank D. Sulla-Menashe and M. Friedl for producing and sharing the MCD12C1 land-cover product. The authors are grateful to P. Jonsson and L. Eklundh for making the TIMESAT software available. The authors also thank A. Zeileis for support with the "bfast" package in R. The authors have no conflict of interests to declare. This work was carried out on the Dutch national e-infrastructure with the support of SURF Cooperative.

DATA ACCESSIBILITY

The R code (R Core Team, 2018) for the new BFAST01 typology is already available by contacting the authors, and the "bfast" package in R is being updated to incorporate the new typology. Raster files with the BFAST01 new typology outputs and the drylands mask used by the authors are available online at <https://doi.org/10.5281/zenodo.3724694>

ORCID

Paulo N. Bernardino  <https://orcid.org/0000-0002-9226-3160>

REFERENCES

- Barbier, N., Couteron, P., Lejoly, J., Deblauwe, V., & Lejeune, O. (2006). Self-organized vegetation patterning as a fingerprint of climate and human impact on semi-arid ecosystems. *Journal of Ecology*, 94, 537–547. <https://doi.org/10.1111/j.1365-2745.2006.01126.x>
- Berdugo, M., Kéfi, S., Soliveres, S., & Maestre, F. T. (2017). Plant spatial patterns identify alternative ecosystem multifunctionality states in global drylands. *Nature Ecology and Evolution*, 1, 0003. <https://doi.org/10.1038/s41559-017-0382-5>
- Castellano, M. J., & Valone, T. J. (2007). Livestock, soil compaction and water infiltration rate: Evaluating a potential desertification recovery mechanism. *Journal of Arid Environments*, 71, 97–108. <https://doi.org/10.1016/j.jaridenv.2007.03.009>
- Center for International Earth Science Information Network (CIESIN). (2017). *Documentation for the gridded population of the world, Version 4 (GPWv4), Revision 10 Data Sets*. Palisades, NY: NASA Socioeconomic Data and Applications Center (SEDAC). <https://doi.org/10.7927/H4639MPP>
- Chapin, F. S., Zavaleta, E. S., Eviner, V. T., Naylor, R. L., Vitousek, P. M., Reynolds, H. L., ... Díaz, S. (2000). Consequences of changing biodiversity. *Nature*, 405(6783), 234–242.
- Cherlet, M., Hutchinson, C., Reynolds, J., Hill, J., Sommer, S., von Maltitz, G., ... Smid, M. (2018). *World atlas of desertification: Rethinking land degradation and sustainable land management* (3rd ed.). Luxembourg: Publication Office of the European Union.
- de Beurs, K. M., & Henebry, G. M. (2004). Land surface phenology, climatic variation, and institutional change: Analyzing agricultural land cover change in Kazakhstan. *Remote Sensing of Environment*, 89, 497–509. <https://doi.org/10.1016/j.rse.2003.11.006>
- de Jong, R., Verbesselt, J., Schaepman, M. E., & de Bruin, S. (2012). Trend changes in global greening and browning: Contribution of short-term trends to longer-term change. *Global Change Biology*, 18, 642–655. <https://doi.org/10.1111/j.1365-2486.2011.02578.x>
- de Jong, R., Verbesselt, J., Zeileis, A., & Schaepman, M. E. (2013). Shifts in global vegetation activity trends. *Remote Sensing*, 5, 1117–1133. <https://doi.org/10.3390/rs5031117>
- De Keersmaecker, W., Lhermitte, S., Tits, L., Honnay, O., Somers, B., & Coppin, P. (2015). A model quantifying global vegetation resistance and resilience to short-term climate anomalies and their relationship with vegetation cover. *Global Ecology and Biogeography*, 24, 539–548. <https://doi.org/10.1111/geb.12279>
- Drummond, M. A., Auch, R. F., Karstensen, K. A., Saylor, K. L., Taylor, J. L., & Loveland, T. R. (2012). Land change variability and human–environment dynamics in the United States Great Plains. *Land Use Policy*, 29, 710–723. <https://doi.org/10.1016/j.landusepol.2011.11.007>
- Easterling, D. R., Meehl, G. A., Parmesan, C., Changnon, S. A., Karl, T. R., & Mearns, L. O. (2000). Climate extremes: Observations, modeling, and impacts. *Science*, 289(5487), 2068–2074. <https://doi.org/10.1126/science.289.5487.2068>
- Elagib, N. A. (2013). Meteorological drought and crop yield in Sub-Saharan Sudan. *International Journal of Water Resources and Arid Environments*, 2, 164–171.

- Elagib, N. A., & Elhag, M. M. (2011). Major climate indicators of ongoing drought in Sudan. *Journal of Hydrology*, 409, 612–625. <https://doi.org/10.1016/j.jhydrol.2011.08.047>
- Fensholt, R., Langanke, T., Rasmussen, K., Reenberg, A., Prince, S. D., Tucker, C., ... Wessels, K. (2012). Greenness in semi-arid areas across the globe 1981–2007 – An Earth Observing Satellite based analysis of trends and drivers. *Remote Sensing of Environment*, 121, 144–158. <https://doi.org/10.1016/j.rse.2012.01.017>
- Fensholt, R., Rasmussen, K., Kaspersen, P., Huber, S., Horion, S., & Swinnen, E. (2013). Assessing land degradation/recovery in the African Sahel from long-term Earth observation based primary productivity and precipitation relationships. *Remote Sensing*, 5, 664–686. <https://doi.org/10.3390/rs5020664>
- Friedl, M., & Sulla-Menasha, D. (2015). MCD12C1 MODIS/Terra+Quia land cover type yearly L3 global 0.05Deg CMG V006. NASA EOSDIS Land Processes DAAC. Retrieved from 28 May 2018. <https://doi.org/10.5067/MODIS/MCD12C1.006>
- Funk, C., Peterson, P., Landsfeld, M., Pedreros, D., Verdin, J., Shukla, S., ... Michaelsen, J. (2015). The climate hazards infrared precipitation with stations—A new environmental record for monitoring extremes. *Scientific Data*, 2, 150026. <https://doi.org/10.1038/sdata.2015.66>
- Herrmann, S. M., Anyamba, A., & Tucker, C. J. (2005). Recent trends in vegetation dynamics in the African Sahel and their relationship to climate. *Global Environmental Change*, 15, 394–404. <https://doi.org/10.1016/j.gloenvcha.2005.08.004>
- Hickler, T., Eklundh, L., Seaquist, J. W., Smith, B., Ardö, J., Olsson, L., ... Sjöström, M. (2005). Precipitation controls Sahel greening trend. *Geophysical Research Letters*, 32, 1–4. <https://doi.org/10.1029/2005GL024370>
- Hölzel, N., Haub, C., Ingelfinger, M. P., Otte, A., & Pilipenko, V. N. (2002). The return of the steppe – Large-scale restoration of degraded land in southern Russia during the post-Soviet era. *Journal for Nature Conservation*, 10, 75–85. <https://doi.org/10.1078/1617-1381-00009>
- Horion, S., Cornet, Y., Erpicum, M., & Tychon, B. (2013). Studying interactions between climate variability and vegetation dynamic using a phenology based approach. *International Journal of Applied Earth Observation and Geoinformation*, 20, 20–32. <https://doi.org/10.1016/j.jag.2011.12.010>
- Horion, S., Ivits, E., De Keersmaecker, W., Tagesson, T., Vogt, J., & Fensholt, R. (2019). Mapping European ecosystem change types in response to land-use change, extreme climate events, and land degradation. *Land Degradation and Development*, 30, 951–963. <https://doi.org/10.1002/ldr.3282>
- Horion, S., Prishchepov, A. V., Verbesselt, J., de Beurs, K., Tagesson, T., & Fensholt, R. (2016). Revealing turning points in ecosystem functioning over the Northern Eurasian agricultural frontier. *Global Change Biology*, 22, 2801–2817. <https://doi.org/10.1111/gcb.13267>
- Huxman, T. E., Smith, M. D., Fay, P. A., Knapp, A. K., Shaw, M. R., Loik, M. E., ... Williams, D. C. (2004). Convergence across biomes to common rain use efficiency. *Nature*, 429, 651–654. <https://doi.org/10.1038/nature02597.1>
- Jax, K. (2005). Function and “functioning” in ecology: What does it mean? *Oikos*, 111, 641–648. <https://doi.org/10.1111/j.1600-0706.2005.13851.x>
- Jönsson, P., & Eklundh, L. (2004). TIMESAT – A program for analyzing time-series of satellite sensor data. *Computers and Geosciences*, 30, 833–845. <https://doi.org/10.1016/j.cageo.2004.05.006>
- Le Houérou, H. N. (1984). Rain use efficiency – A unifying concept in arid-land ecology. *Journal of Arid Environments*, 7, 213–247.
- Lenton, T. M., Held, H., Kriegler, E., Hall, J. W., Lucht, W., Rahmstorf, S., & Schellnhuber, H. J. (2008). Tipping elements in the Earth's climate system. *Proceedings of the National Academy of Sciences USA*, 105, 1786–1793. <https://doi.org/10.1073/pnas.0911106106>
- Lotsch, A., Friedl, M. A., Anderson, B. T., & Tucker, C. J. (2005). Response of terrestrial ecosystems to recent Northern Hemispheric drought. *Geophysical Research Letters*, 32(6), 1–5. <https://doi.org/10.1029/2004GL022043>
- Millennium Ecosystem Assessment. (2005). *Ecosystems and human well-being: Desertification synthesis*. Washington, DC: World Resources Institute.
- Nemani, R. R., Keeling, C. D., Hashimoto, H., Jolly, W. M., Piper, S. C., Tucker, C. J., ... Running, S. W. (2003). Climate-driven increases in global terrestrial net primary production from 1982 to 1999. *Science*, 300, 1560–1564. <https://doi.org/10.1126/science.1082750>
- Peel, M. C., Finlayson, B. L., & McMahon, T. A. (2007). Updated world map of the Köppen-Geiger climate classification. *Hydrology and Earth System Sciences*, 11, 1633–1644. <https://doi.org/10.5194/hess-11-1633-2007>
- Ponce-Campos, G. E., Moran, M. S., Huete, A., Zhang, Y., Bresloff, C., Huxman, T. E., ... Starks, P. J. (2013). Ecosystem resilience despite large-scale altered hydroclimatic conditions. *Nature*, 494(7437), 349–352. <https://doi.org/10.1038/nature11836>
- Prince, S. D., Wessels, K. J., Tucker, C. J., & Nicholson, S. E. (2007). Desertification in the Sahel: A reinterpretation of a reinterpretation. *Global Change Biology*, 13, 1308–1313. <https://doi.org/10.1111/j.1365-2486.2007.01356.x>
- R Core Team. (2018). *R: A language and environment for statistical computing*. Vienna, Austria: R Foundation for Statistical Computing. Retrieved from <https://www.r-project.org/>
- Rasmussen, K., D'haen, S., Fensholt, R., Fog, B., Horion, S., Nielsen, J. O., ... Reenberg, A. (2016). Environmental change in the Sahel: Reconciling contrasting evidence and interpretations. *Regional Environmental Change*, 16, 673–680. <https://doi.org/10.1007/s10113-015-0778-1>
- Reynolds, J. F., Smith, D. M. S., Lambin, E. F., Turner, B. L., Mortimore, M., Batterbury, S. P. J., ... Walker, B. (2007). Global desertification: Building a science for dryland development. *Science*, 316(5826), 847–851. <https://doi.org/10.1126/science.1131634>
- Rice, K. J., Matzner, S. L., Byer, W., & Brown, J. R. (2004). Patterns of tree dieback in Queensland, Australia: The importance of drought stress and the role of resistance to cavitation. *Oecologia*, 139, 190–198. <https://doi.org/10.1007/s00442-004-1503-9>
- Scheffer, M., Carpenter, S., Foley, J. A., Folke, C., & Walker, B. (2001). Catastrophic shifts in ecosystems. *Nature*, 413(6856), 591–596. <https://doi.org/10.1038/35098000>
- Scholes, R., Montanarella, L., Brainich, A., Barger, N., ten Brink, B., Cantele, M., ... Willems, L. (2018). *Summary for policymakers of the thematic assessment report on land degradation and restoration of the intergovernmental science-policy platform on biodiversity and ecosystem services* (pp. 1–44). Bonn, Germany: IPBES Secretariat.
- Sullivan, P., Hellerstein, D., Hansen, L. R., Johansson, R., Koenig, S., Lubowski, R. N., ... Bucholz, S. (2004). The conservation reserve program: Economic implications for rural America. *Agricultural Economic Report Number*, 834, 112. Retrieved from <https://www.ers.usda.gov/publications/pub-details/?pubid=41678>
- Tian, F., Fensholt, R., Verbesselt, J., Grogan, K., Horion, S., & Wang, Y. (2015). Evaluating temporal consistency of long-term global NDVI datasets for trend analysis. *Remote Sensing of Environment*, 163, 326–340. <https://doi.org/10.1016/j.rse.2015.03.031>
- Tucker, C. J. (1979). Red and photographic infrared linear combinations for monitoring vegetation. *Remote Sensing of Environment*, 8, 127–150. [https://doi.org/10.1016/0034-4257\(79\)90013-0](https://doi.org/10.1016/0034-4257(79)90013-0)
- Tucker, C. J., Pinzon, J. E., Brown, M. E., Slayback, D. A., Pak, E. W., Mahoney, R., ... El Saleous, N. (2005). An extended AVHRR 8-km NDVI dataset compatible with MODIS and SPOT vegetation NDVI data. *International Journal of Remote Sensing*, 26, 4485–4498. <https://doi.org/10.1080/01431160500168686>
- Verbesselt, J., Hyndman, R., Newnham, G., & Culvenor, D. (2010). Detecting trend and seasonal changes in satellite image time series. *Remote Sensing of Environment*, 114, 106–115. <https://doi.org/10.1016/j.rse.2009.08.014>

- Vicente-Serrano, S. M., Beguería, S., López-Moreno, J. I., Angulo, M., & El Kenawy, A. (2010). A new global 0.5° gridded dataset (1901–2006) of a multiscalar drought index: Comparison with current drought index datasets based on the Palmer Drought Severity Index. *Journal of Hydrometeorology*, 11, 1033–1043. <https://doi.org/10.1175/2010JHM1224.1>
- Vicente-Serrano, S. M., Gouveia, C., Camarero, J. J., Begueria, S., Trigo, R., Lopez-Moreno, J. I., ... Sanchez-Lorenzo, A. (2013). Response of vegetation to drought time-scales across global land biomes. *Proceedings of the National Academy of Sciences USA*, 110, 52–57. <https://doi.org/10.1073/pnas.1207068110>
- Witt, G. B., Harrington, R. A., & Page, M. J. (2009). Is “vegetation thickening” occurring in Queensland’s mulga lands? A 50-year aerial photographic analysis. *Australian Journal of Botany*, 57, 572–582. <https://doi.org/10.1071/BT08217>
- Witt, G. B., Noël, M. V., Bird, M. I., Beeton, R. J. S., & Menzies, N. W. (2011). Carbon sequestration and biodiversity restoration potential of semi-arid mulga lands of Australia interpreted from long-term grazing exclosures. *Agriculture, Ecosystems and Environment*, 141(1–2), 108–118. <https://doi.org/10.1016/j.agee.2011.02.020>
- Zonn, I. S. (1995). Desertification in Russia: Problems and solutions (an example in the Republic of Kalmykia-Khalmg Tangch). *Environmental Monitoring and Assessment*, 37(1–3), 347–363. <https://doi.org/10.1007/BF00546900>

BIOSKETCH

The research team focuses on better understanding of turning points in dryland ecosystem functioning by combining advanced Earth observation techniques with dynamic vegetation models. More information can be found at <http://uturndryland.wixsite.com/uturn>

SUPPORTING INFORMATION

Additional supporting information may be found online in the Supporting Information section.

How to cite this article: Bernardino PN, De Keersmaecker W, Fensholt R, Verbesselt J, Somers B, Horion S. Global-scale characterization of turning points in arid and semi-arid ecosystem functioning. *Global Ecol Biogeogr*. 2020;29: 1230–1245. <https://doi.org/10.1111/geb.13099>